Molecular and Ionic Interaction with Graphene Nanoflakes: A Computational Investigation of CO2, H2O, Li, Mg, Li+, and Mg2+ Interaction with Polycyclic Aromatic Hydrocarbons

ARTICLE *in* THE JOURNAL OF PHYSICAL CHEMISTRY C · APRIL 2011

Impact Factor: 4.77 · DOI: 10.1021/jp201578p

2 AUTHORS:

Deivasigamani Umadevi
Trinity College Dublin
13 PUBLICATIONS **154** CITATIONS
SEE PROFILE

G Narahari Sastry
Indian Institute of Chemical Technology
262 PUBLICATIONS **5,299** CITATIONS
SEE PROFILE

THE JOURNAL OF PHYSICAL CHEMISTRY C

ARTICLE

pubs.acs.org/JPCC

Molecular and Ionic Interaction with Graphene Nanoflakes: A Computational Investigation of CO_2, H_2O, Li, Mg, Li^+, and Mg^{2+} Interaction with Polycyclic Aromatic Hydrocarbons

Deivasigamani Umadevi and G. Narahari Sastry*

Molecular Modeling group, Indian Institute of Chemical Technology, Tarnaka, Hyderabad - 500 607, India

Supporting Information

ABSTRACT: Understanding the nature of nonbonded interactions on the graphene surface is a problem of outstanding interest. Highly reliable M05-2X/6-311++G**//M05-2X/6-31G* DFT calculations were performed to understand the interaction of small molecules and ionic species with graphenes. Various linear and branched polycyclic aromatic hydrocarbons (PAHs) were taken as models of the graphene surface, and their interaction with small molecules (CO_2 and H_2O), metal atoms (Li and Mg), and metal ions (Li^+ and Mg^{2+}) has been studied. The effect of ring size is found to be profound on the interaction energy values and shows an interesting contrast with various species. Our results indicate that the metal atoms and ions are chemisorbed, while CO_2 and H_2O are physisorbed on the PAH surface. H_2O displays a stronger affinity for complexation compared to CO_2. The binding strength of the molecules has been correlated with the nucleus independent chemical shift (NICS), a local aromaticity index, highest occupied molecular orbital (HOMO) energy, and polarizability of PAHs.

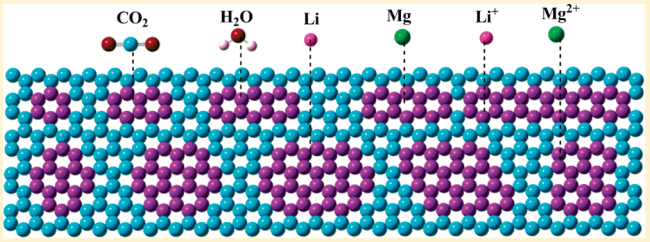

INTRODUCTION

Graphene, the youngest of carbon allotropes, is a planar form of carbon atoms packed in a two-dimensional hexagonal lattice. Its extended honeycomb network is the basic building block of other important allotropes such as 3D graphite, which is formed by the stacking of several layers of graphene, 1D nanotube, which is nothing but the rolled form of graphene and the 0D fullerene which is formed by wrapped graphenes.[1] Graphene is also a promising candidate in the designing of new nanomaterials for energy storage devices, fuel cells and biosensors due to its high stability, elasticity and electromechanical modulation.[2] Moreover, graphene shows extraordinary electronic properties compared to many of the conventional materials; the highly conductive graphene becomes an insulator after hydrogenation. This hydrogenation of graphene is highly reversible; the intrinsic conductivity as well as the structure of graphene can be restored by annealing.[3] Graphene has become an important material in nanoscale electronics because of its compatibility with industry-standard lithographic processing, electron mobilities up to 150 times greater than Si, and a thermal conductivity twice that of diamond.[4] Doping of graphene with various atoms and molecules is one of the ways to control the properties of graphene based electronics. The adsorbed species can change the electronic and magnetic properties of the graphene through various types of interactions.[5]

Development of sensors based on graphene is an area of recent interest. The structure and physical properties of graphene make it a promising candidate as a sensor to detect different gases such as H_2, NO_2, and NH_3. Scheden et al., in their recent experimental results, stated that graphene based sensors allow the ultimate sensitivity such that the adsorption of individual gas molecules could be detected.[6] Graphene−polyaniline nanocomposite is found to be a good sensor for H_2 gas, and nitrogen doped graphene is found to have application in electrochemical biosensing.[7] It is also shown that the properties of graphene can be modified through functionalization. Intentional functionalization of graphene with hydrogen, oxygen, or other chemical groups is of great interest as a way to engineer the different properties of graphene. A recent study reveals that graphene with controlled epoxide functionalization can be used as a starting material for diverse chemical functionalization by chemical modification of the epoxide group. The functionalization of graphene and single-walled carbon nanotubes with individual 3d transition metal atoms was also modeled using density functional theory calculations.[8,9] Graphene nanoflakes are finite-sized graphene in both dimensions which are none other than the larger PAHs. These PAHs themselves are of great research interest due to their high stability, their rigid planar structure, and their characteristic optical spectra.[10] Numerous studies have been performed with PAHs to model the graphene surface. Podeszwa deduced the interactions of graphene sheets from the properties of PAHs and reported that the extrapolated

Received: February 17, 2011
Revised: April 18, 2011
Published: April 28, 2011

Scheme 1. Linear (L*n*) and Branched (B*n*) Polycyclic Aromatic Hydrocarbons

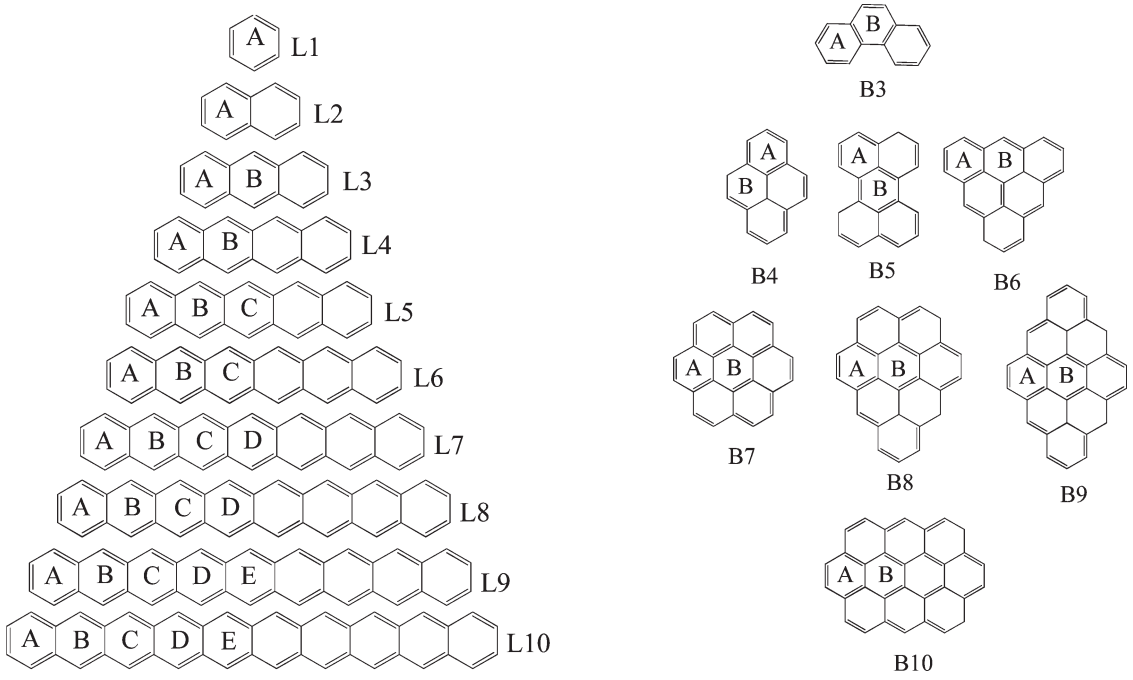

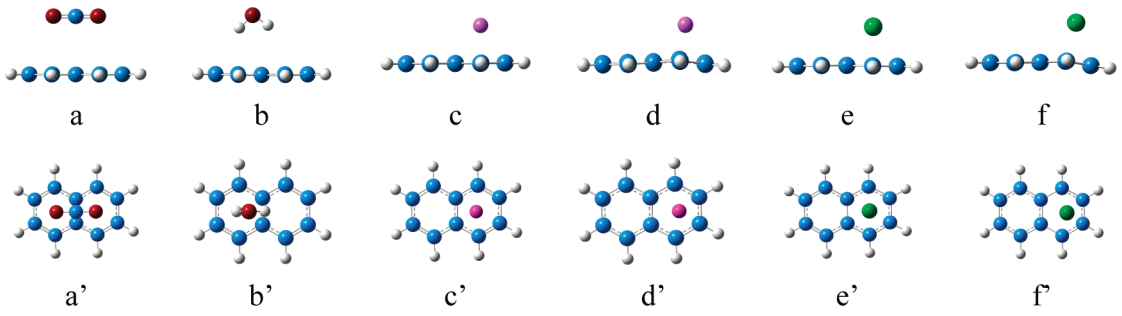

Figure 1. Mode of interaction of (a, a′) CO_2, (b, b′) H_2O, (c, c′) Li^+, (d, d′) Li, (e, e′) Mg^{2+}, and (f, f′) Mg with PAHs. The side and front views are given in the first and second rows, respectively.

physical picture of graphene−graphene interaction is very similar to that of the stacked PAHs.[11] Understanding the interaction of alkali and alkaline earth metals like Li, Mg, etc., with graphene is important because of their potential applications in lithium-based batteries, alkali-metal doped hydrogen storage devices, and alkali-metal containing superconductors, and since Li and other alkali metals are lighter, cheaper, and less reactive, they are considered to be better dopants than transition metals.[12] Metal ions such as Li^+ and Mg^{2+} form cation−π type complexes with graphene, and we have done various studies on cation−π interactions in order to understand its significance in biological processes and also in designing new energy storage materials.[13] The effect of increasing the size of the π-system on the strength of the cation−π interaction has been studied extensively.[14] Moreover, a detailed study on the solvation effect on cation−π interaction reveals that solvation of the metal ion decreases its interaction with the π-system, while the solvation of the π- system increases its interaction with the metal ion.[15] CO_2 evolves as a byproduct in the production of H_2 gas from methane, and it has to be selectively removed from the mixture; hence, understanding the interaction of CO_2 with graphene is of fundamental importance, as it is useful in designing novel materials for the CO_2 capture and storage which is also a recent crucial environmental problem to be solved. Similarly, there has been considerable interest in graphene−H_2O interaction after the discovery that water can fill carbon nanotubes and also it was shown that graphene possesses good sorption properties toward various small molecules such as CO_2 and H_2.[16] Besides, graphene seems to be a promising material for biological and medicinal applications. Liu and co-workers have found that the interaction between the aromatic drug molecules and the nanographene sheets is simple noncovalent adsorption interaction.[17,18] Thus, the study of noncovalent interaction with graphene sheet becomes important.

The foregoing analysis clearly indicates the fundamental importance of understanding the interactions on the graphene surface. In the present study, we have undertaken the study of the nonbonded interaction involving CO_2, H_2O, Li, Mg, Li^+, and Mg^{2+} with various model systems aimed to mimic the graphene surface. CO_2 and H_2O are examples for the prototypical hydrophobic and

dx.doi.org/10.1021/jp201578p |*J. Phys. Chem. C* 2011, 115, 9656–9667

Table 1. The Principal Geometric Parameters (r in Å) Obtained at the M05-2X/6-31G* Level of the Complexes Formed between Linear PAHs (Ln) with CO_2, H_2O, Li^+, Mg^{2+}, Li, and Mg

		linear polycyclic aromatic hydrocarbon									
	ring	L1	L2	L3	L4	L5	L6	L7	L8	L9	L10
CO_2	A	3.099	3.140	3.068	3.045	3.021	3.058	3.056	3.058	3.056	3.054
	B			3.134	3.131	3.134	3.133	3.120	3.135	3.134	3.149
	C					3.125	3.126	3.125	3.126	3.132	3.127
	D							3.125	3.125	3.125	3.125
	E									3.123	3.122
H_2O	A	3.172	3.181	3.194	3.180	3.184	3.181	3.179	3.178	3.178	3.177
	B			3.194	3.221	3.219	3.214	3.204	3.205	3.203	3.208
	C					3.216	3.218	3.206	3.211	3.221	3.236
	D								3.227	3.219	3.206
	E									3.221	3.209
Li^+	A	1.874	1.853	1.838	1.829	1.824	1.820	1.818	1.816	1.816	1.816
	B			1.838	1.829	1.822	1.818	1.817	1.814	1.813	1.792
	C					1.821	1.816	1.815	1.812	1.809	1.797
	D							1.812	1.808	1.807	1.811
	E									1.806	1.886
Mg^{2+}	A	1.937	1.891	1.862	1.845	1.834	1.827	1.847	1.845	1.843	1.841
	B			1.866	1.850	1.838	1.824	1.822	1.819	1.818	1.817
	C					1.838	1.815	1.810	1.807	1.806	1.857
	D								1.802	1.799	1.877
	E									1.982	1.900
Li	A	2.272	1.735	1.717	1.716	1.718	1.720	1.722	1.723	1.725	1.728
	B			1.719	1.726	1.730	1.731	1.733	1.734	1.735	1.734
	C					1.732	1.736	1.737	1.738	1.740	1.743
	D							1.739	1.740	1.742	1.752
	E									1.754	1.762
Mg	A	1.986	2.083	2.064	2.055	2.050	2.048	3.421	3.428	2.431	2.043
	B			2.037	2.046	2.048	2.049	2.050	2.051	2.109	2.166
	C					2.049	2.052	2.054	2.055	2.055	2.137
	D								2.056	2.057	2.169
	E									2.626	2.231

Table 2. The Principal Geometric Parameters (r in Å) Obtained at the M05-2X/6-31G* Level of the Complexes Formed between Branched PAHs (Bn) with CO_2, H_2O, Li^+, Mg^{2+}, Li, and Mg

		branched polycyclic aromatic hydrocarbon							
	ring	B3	B4	B5	B6	B7	B8	B9	B10
CO_2	A	3.105	3.035	3.093	3.084	3.080	3.047	3.023	3.109
	B	3.112	3.116	3.078	3.047	3.105	3.095	3.097	3.116
H_2O	A	3.191	3.176	3.211	3.034	3.200	3.175	3.158	3.180
	B	3.192	3.167	3.149	3.143	3.176	3.185	3.194	3.218
Li^+	A	1.843	1.838	1.832	1.839	1.831	1.827	1.836	1.823
	B	1.841	1.845	1.843	1.877	1.849	1.836	1.830	1.834
Mg^{2+}	A	1.883	1.867	1.865	2.556	1.843	2.428	2.007	1.837
	B	1.851	1.850	1.861	2.327	1.822	1.820	1.834	1.818
Li	A	1.746	1.706	1.721	1.722	1.724	1.736	1.743	1.730
	B	1.709	1.723	1.729	1.760	1.747	1.758	1.754	1.756
Mg	A	2.073	2.046	2.071	2.211	2.209	2.187	2.126	2.048
	B	2.460	1.140	2.048	3.431	2.207	2.091	2.109	2.081

hydrophilic surfaces. The interaction of neutral Li and Mg atoms is another class, and their charge transfer interaction is important. The third type, Li^+ and Mg^{2+}, provide examples for cation−π interactions which generated tremendous interest in recent years. The present study aims to provide a comprehensive and comparative analysis of these three different types of issues on the graphene surface. The orientation of these species and their binding strength with the model PAHs have been quantum chemically estimated. The interaction energy of the complexes at various sites on the PAH surface is analyzed with the aim of understanding the feasibility and conformational preference of these molecules and ions on the graphene model systems. We have also correlated the polarizability, HOMO energy, and NICS value of the PAHs with the observed binding energy. The reorganization energy of the PAHs in the complexed state and the charge transferred during the complex formation are also addressed.

COMPUTATIONAL DETAILS

All the structures were subjected to full geometry optimizations without any constraints at the M05-2X/6-31G* level of

Table 3. Interaction Energy (IE in kcal/mol) of Linear PAHs (L*n*) with CO_2, H_2O, Li^+, Mg^{2+}, Li, and Mg at the M05-2X/6-311++G//M05-2X/6-31G* Level**

		linear polycyclic aromatic hydrocarbon									
	ring	L1	L2	L3	L4	L5	L6	L7	L8	L9	L10
CO_2	A	−2.37	−2.71	−2.71	−2.72	−2.64	−2.67	−2.71	−2.74	−2.70	−2.90
	B			−2.72	−2.76	−2.81	−2.80	−2.85	−2.88	−2.84	−3.00
	C					−2.67	−2.83	−2.86	−2.89	−2.92	−3.01
	D							−2.94	−2.91	−2.87	−3.05
	E									−2.89	−3.06
H_2O	A	−4.19	−5.05	−4.94	−4.95	−4.90	−4.89	−4.88	−4.90	−4.84	−5.00
	B			−4.94	−4.94	−4.87	−4.85	−4.84	−4.86	−4.74	−4.88
	C					−4.79	−4.79	−4.78	−4.80	−4.68	−4.78
	D							−4.74	−4.76	−4.63	−4.70
	E									−4.62	−4.65
Li^+	A	−41.68	−44.34	−46.36	−47.76	−48.67	−49.30	−49.75	−50.06	−50.21	−50.47
	B			−46.34	−47.97	−49.16	−49.95	−50.60	−50.93	−51.14	−39.69
	C					−49.39	−50.49	−51.18	−51.71	−52.04	−40.31
	D							−51.48	−52.13	−52.60	−39.19
	E									−52.85	−37.47
Mg^{2+}	A	−122.68	−138.52	−149.83	−157.75	−163.26	−167.15	−170.02	−172.13	−173.64	−174.95
	B			−149.32	−158.23	−164.71	−169.29	−172.68	−174.99	−176.66	−178.04
	C					−165.57	−171.12	−175.12	−178.01	−180.02	−216.02
	D							−176.03	−179.73	−182.24	−214.36
	E									−203.92	−213.23
Li	A	−2.82	−22.87	−31.47	−37.00	−40.47	−42.66	−44.18	−45.08	−45.70	−46.20
	B			−32.57	−39.39	−43.63	−46.34	−47.99	−49.23	−49.79	−56.35
	C					−44.76	−48.27	−50.48	−51.96	−52.85	−58.06
	D							−51.31	−53.25	−54.46	−58.33
	E									−54.94	−57.81
Mg	A	−16.33	−44.10	−51.24	−55.76	−58.66	−60.46	−61.34	−61.53	−62.81	−63.12
	B			−52.59	−58.73	−62.43	−64.71	−66.28	−67.19	−69.50	−78.98
	C					−63.87	−67.01	−68.92	−70.28	−71.00	−81.60
	D							−69.51	−71.61	−72.70	−80.50
	E									−81.94	−80.70

Table 4. Interaction Energy (IE in kcal/mol) of Branched PAHs (B*n*) with CO_2, H_2O, Li^+, Mg^{2+}, Li, and Mg at the M05-2X/6-311++G//M05-2X/6-31G* Level**

		branched polycyclic aromatic hydrocarbon							
	ring	B3	B4	B5	B6	B7	B8	B9	B10
CO_2	A	−2.60	−3.08	−3.23	−3.30	−2.58	−2.48	−3.02	−3.41
	B	−2.85	−3.44	−3.50	−3.85	−3.37	−3.20	−3.49	−3.70
H_2O	A	−4.91	−4.89	−4.87	−6.74	−4.65	−4.71	−4.57	−4.71
	B	−4.90	−4.69	−4.98	−6.61	−4.63	−4.66	−4.66	−4.67
Li^+	A	−46.82	−47.83	−48.95	−65.40	−48.95	−49.90	−49.12	−51.11
	B	−45.55	−45.61	−45.50	−57.45	−46.56	−47.97	−49.78	−48.79
Mg^{2+}	A	−147.90	−154.13	−160.35	−203.50	−163.23	−178.92	−172.97	−171.99
	B	−149.65	−151.38	−161.18	−202.45	−161.75	−166.71	−169.55	−170.26
Li	A	−20.50	−26.77	−34.22	−80.80	−20.46	−15.94	−38.25	−27.68
	B	−20.09	−24.88	−31.92	−76.80	−15.70	−12.35	−37.19	−27.21
Mg	A	−41.68	−46.04	−52.98	−108.83	−40.49	−42.18	−56.68	−45.06
	B	−41.65	−44.75	−49.23	−108.82	−31.72	−33.97	−53.74	−43.76

theory. This method was chosen, as it appears to be better compared to the more popular B3LYP alternatives when modeling nonbonding interactions.[19] The geometries were optimized using berny optimization and the convergence

dx.doi.org/10.1021/jp201578p |J. Phys. Chem. C 2011, 115, 9656–9667

criteria (the convergence on the rms density matrix is 1.00D-08 hartree, the convergence on the MAX density matrix is 1.00D-06 hartree, and the convergence on energy is 1.00D-06 hartree). All stationary points were characterized as minima after verifying the presence of all real frequencies. Single point energy evaluations were carried out at the M05-2X/6-311++G** level. The interaction energy (IE) was calculated, using eq 1, as the difference between the total energy of the complex (E_{PAH_X}) and the sum of the total energies of the parent PAH (E_{PAH}) and the complex counterparts X (E_X) (where X = CO_2, H_2O, Li^+, Mg^{2+}, Li, and Mg).

$$IE = E_{PAH\_X} - (E_{PAH} + E_X) \quad (1)$$

The interaction energy was corrected for basis set superposition error (BSSE) using the counterpoise correction (CP) scheme proposed by Boys and Bernardi, which is within 1 kcal/mol. However, the binding with the neutral Li and Mg are stronger and could not be treated as nonbonded and thus BSSE correction is not appropriate. Thus, to maintain uniformity, we provided all the results without correction for the BSSE (see the Supporting Information).

NICS[20] calculations were carried out at the M05-2X/6-31G* level of theory, in order to characterize the aromatic nature of all the individual rings of the systems considered in this study. The NICS parameter, which is defined as the absolute value of shielding, is typically computed at the ring center or at any other point of interest of the systems considered. In the current study, the gauge-independent atomic orbital (GIAO) method has been used to perform calculations of the NICS parameters at ring centers determined by the nonweighted mean of the heavy atom coordinates. The negative value of the NICS parameter denotes the aromaticity of the system. The higher the negative value of NICS, the higher is the aromaticity, whereas a positive value of NICS denotes the antiaromaticity of the system.

Polarizability is a measure of the ability of a molecule to respond to an electric field. When a molecule is subjected to an external electric field, some of its electrons acquire sufficient energy to move along the direction of the field. The average molecular polarizability[21] ($\acute{\alpha}$) was calculated as

$$\acute{\alpha} = (\alpha_{xx} + \alpha_{yy} + \alpha_{zz})/3$$

where α_{xx}, α_{yy}, and α_{zz} are the diagonal components of the polarizability tensor.

The PAHs were found to undergo considerable deformation upon complexation with the metal ions, and hence, we

Table 5. Polarizability (au^3) of Linear (L*n*) and Branched (B*n*) Polycyclic Aromatic Hydrocarbons Calculated at the M05-2X/6-31G* Level

system	polarizability	system	polarizability
L1	53.360	B3	140.402
L2	95.921	B4	164.018
L3	148.510	B5	212.794
L4	210.815	B6	568.298
L5	282.043	B7	254.000
L6	361.307	B8	307.144
L7	447.587	B9	384.990
L8	539.754	B10	365.662
L9	637.108		
L10	738.805		

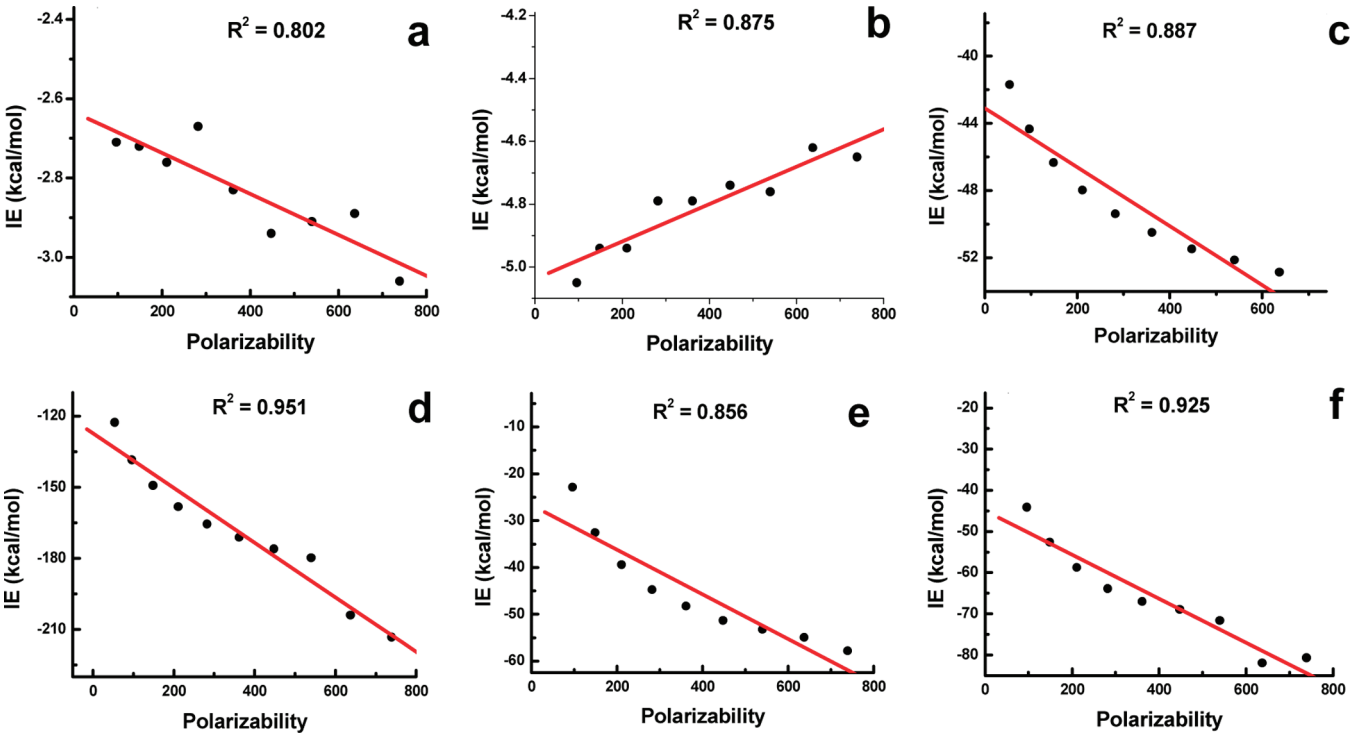

Figure 2. Correlation between the polarizability value (au^3) of linear PAHs (L*n*) and the interaction energy (kcal/mol) of their complexes with (a) CO_2, (b) H_2O, (c) Li^+, (d) Mg^{2+}, (e) Li, and (f) Mg at the M05-2X/6-311++G**//M05-2X/6-31G* level of theory.

dx.doi.org/10.1021/jp201578p |J. Phys. Chem. C 2011, 115, 9656–9667

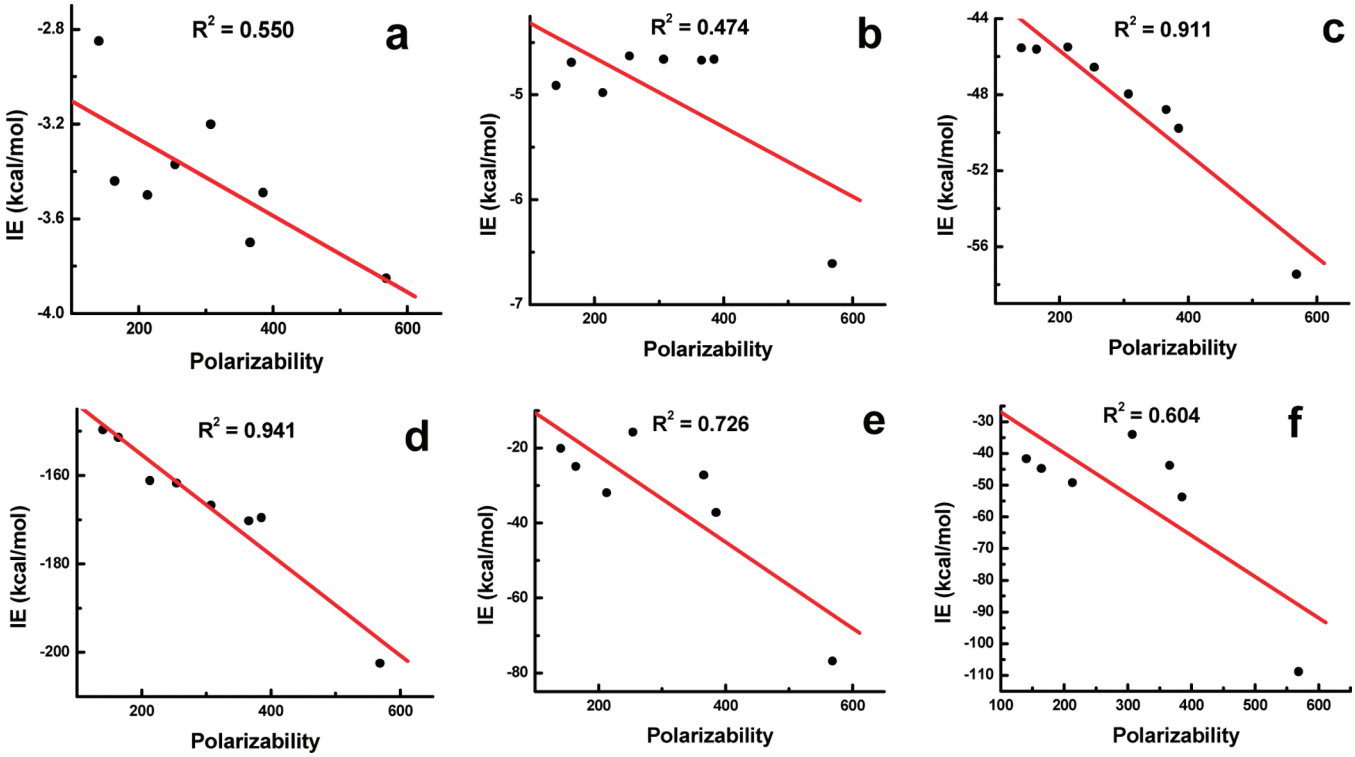

Figure 3. Correlation between the polarizability value (au^3) of branched PAHs (B*n*) and interaction energy (kcal/mol) of their complexes with (a) CO_2, (b) H_2O, (c) Li^+, (d) Mg^{2+}, (e) Li, and (f) Mg at the M05-2X/6-311++G**//M05-2X/6-31G* level.

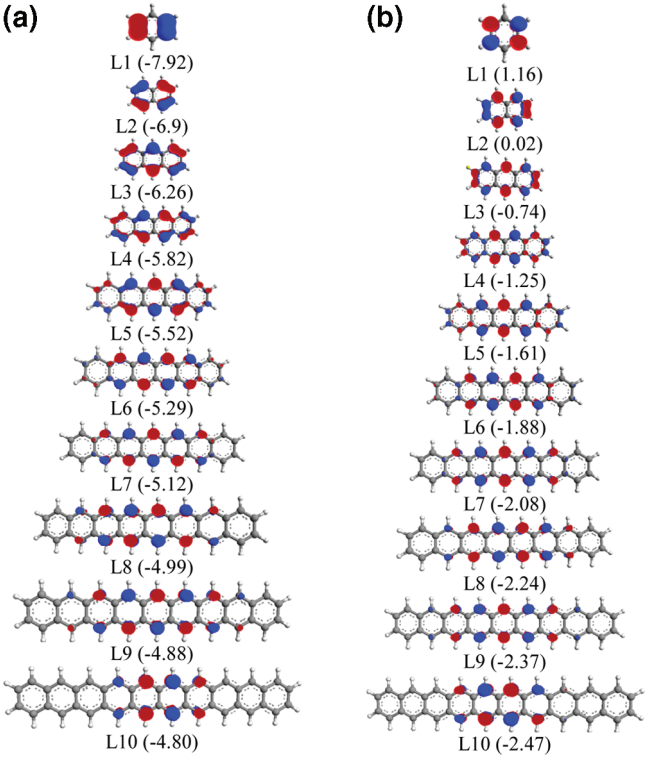

Figure 4. Orbital patterns of the (a) HOMO and (b) LUMO of the linear PAHs (L*n*) with their corresponding energy values (eV) at the M05-2X/6-31G* level.

have calculated the reorganization energy (RE), which is the difference in the energy of a system in the complexed state and in the free state.

$$\mathrm{RE} = E_{(\mathrm{PAH\ in\ complex})} - E_{(\mathrm{PAH})}$$

The natural bond orbital (NBO) charges of all the systems considered were calculated at the M05-2X/6-311++G** level.[22] All the calculations were done in the Gaussian 03, revision E.01, suite of programs.[23]

RESULTS AND DISCUSSION

In this paper, we have chosen two classes of PAHs to model the graphene surface, as illustrated in Scheme 1. The first class is the linear PAHs in which the benzene rings are linearly fused (also called polyacenes), and the second class is the nonlinearly fused benzene rings which are referred to as branched PAHs throughout the manuscript.

The nomenclature used in this discussion is L*n* ($n = 1, 2 \ldots 10$) for the linear PAHs, where L represents the linearly fused PAHs and *n* represents the number of benzene rings present in a given PAH. Similarly, the branched PAHs are named as B*n* ($n = 3-10$). The peripheral ring in each PAH is termed as A, and the successive rings are termed as B, C, D, and so on, as shown in Scheme 1. In this study, we have considered the π complexes formed by these PAHs with various species such as CO_2, H_2O, Li^+, Mg^{2+}, Li, and Mg. The complex counterparts are classified into three types as molecules (CO_2, H_2O), atoms (Li, Mg), and ions (Li^+, Mg^{2+}).

Structure and Binding Energy. Various possible orientations of the complex counterparts with the PAHs were considered, and only the minimum energy orientations were reported. It is found from our calculations that the CO_2 has a parallel mode of orientation, as shown in Figure 1. The C atom in the CO_2 is exactly above the double bond which connects two successive

dx.doi.org/10.1021/jp201578p |J. Phys. Chem. C 2011, 115, 9656–9667

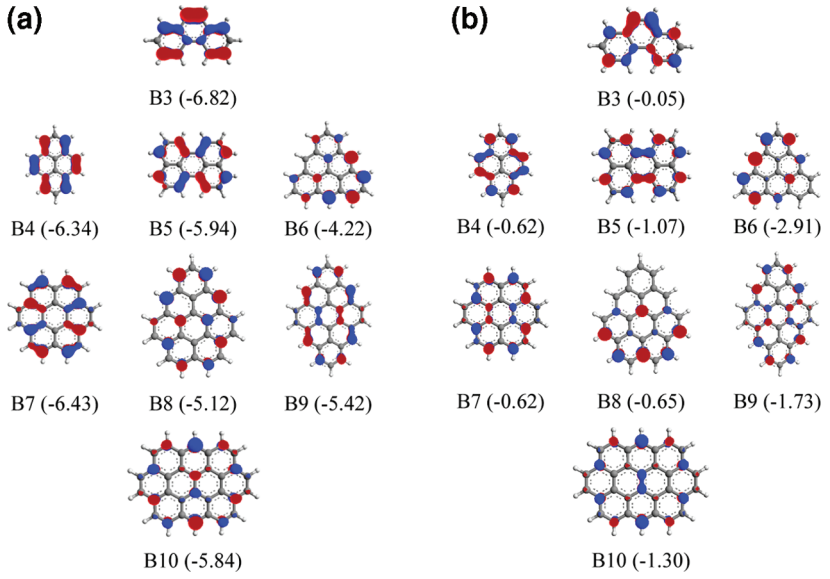

Figure 5. Orbital patterns of the (a) HOMO and (b) LUMO of the branched PAHs (B*n*) with their corresponding energy values (eV) at the M05-2X/6-31G* level.

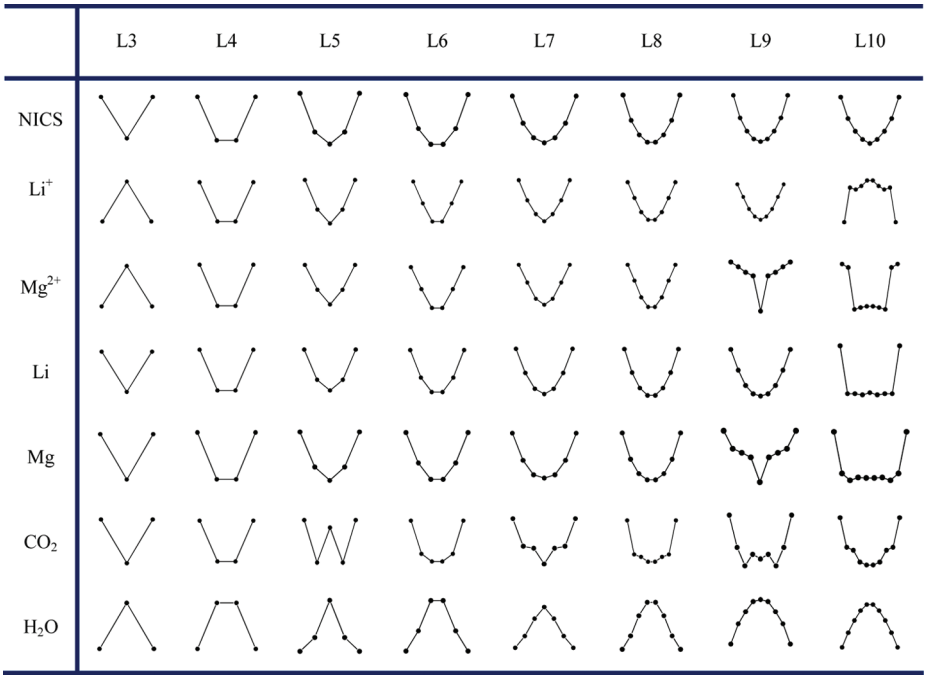

Figure 6. Schematic representation of the comparison of interaction energy trends at each ring in linear PAHs (L*n*) with the NICS value at the M05-2X/6-311++G**//M05-2X/6-31G* level.

rings in the PAHs. The mode of interaction in H_2O is such that it is oriented above the plane of PAHs with the two O−H groups pointing toward the plane. This is in contrast to the orientation of metal ions, which are disposed above the six membered rings, as has been observed before.[14]

The principal geometric parameters (*r*) obtained at the M05-2X/6-31G* level are given in Tables 1 and 2. The *r* values are the nearest distance between the complex counterpart and the plane of the graphene surface. In the case of CO_2, the distance is measured from the C atom of the CO_2 to the graphene surface, while, in the case of H_2O, it is measured from the O atom. Our calculations show that both CO_2 and H_2O are at a distance of around 3.0 Å from the graphene surface. The optimized structures of the alkali metal complexes show that Li^+ and Mg^{2+} are at a distance of around 1.8 Å. In their neutral forms, Li is at a distance of around 1.7 Å, while the Mg is around 2 Å from the PAH surface.

The interaction energies of L*n* and B*n* complexes at the M05-2X/6-31G* level are shown in Tables 3 and 4, respectively. As we can see, the CO_2 complexes have interaction energies in the range around −2.0 kcal/mol, while H_2O complexes have slightly higher interaction energies which are in the range of about −4.0

kcal/mol. Therefore, from our calculations, we can predict that graphene will be more selective toward H_2O than CO_2. However, there is no significant change in the IE values as the size of the PAHs increases, in both the cases of CO_2 and H_2O. Alkali metal ions Li^+ and Mg^{2+} formed complexes with higher interaction energy which are in the range from −37.47 to −52.67 kcal/mol and from −122.68 to −216.02 kcal/mol, respectively. These large values may be due to the charge transfer between the alkali metal cations and the graphene surface. Moreover, as the number of the rings increases, i.e., if we move from L1 to L10, the interaction energy also increases. This is in good agreement with our previous work, where we have studied the size dependence of the π systems on cation−π binding.[14] However, in the case of a branched system, there is no linear increase in the IE as the size of the system increases. Nevertheless, the HOMO energy value and the polarizability value of the PAHs seemed to be strongly correlated with the IE values in the case of B*n* as well as the L*n* systems. A detailed discussion about the HOMO energy value and the polarizability value is given in the later part of this manuscript. The complexes of alkali metal atoms show slightly lesser IE energy than their ionic counterparts; however, they follow the same trend in the IE as that of the alkali metal ions. In the case of Mg atom, as there are two possible spin orientations such as singlet (MgS) and triplet (MgT), we have calculated the interaction energies of both the complexes. Our calculations show that, although MgT is less stable than MgS, it forms complexes with higher binding energy than MgS and hence we have considered the triplet Mg complexes for all the discussions, unless otherwise mentioned.

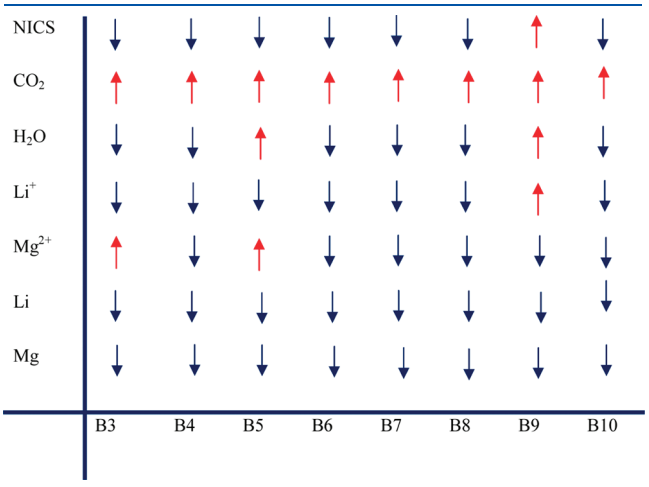

Figure 7. Schematic representation of the comparison of interaction energy trends at each ring in branched polycyclic aromatic hydrocarbon with the NICS value at the M05-2X/6-311++G**//M05-2X/6-31G* level. (Red upward arrows indicate the preference for central rings, and blue downward arrows indicate the preference for peripheral rings.)

In general, the order of magnitude of physisorption energy is defined as lower than about 5 kcal/mol, while that of chemisorption energy is higher than about 12 kcal/mol.[24] Hence, from our numerical study, we can say that CO_2 and H_2O interact with the PAH surfaces by physisorption, whereas the metal atoms and ions interact by chemisorption. Thus, in the case of CO_2 and H_2O complexes, as it is physisorption, there is no appreciable change in the binding energy as the size of the system increases and also in different rings of the same system.

Polarizability. For L*n* complexes of metal ions and atoms, there is a good correlation between the number of fused rings (*n*) and the strength of interaction; the interaction energy of the system increases as the number of fused rings increases. For instance, if we consider all "A" rings in L*n*−Li^+ complexes, the IE increases from L1 to L10. However, it is not the case in B*n* complexes. There is hardly any correlation between the IE and the number of fused rings in the case of B*n*. Among the B*n* system, the B6 system shows maximum interaction energy in complexes with all the counterparts. To understand the origin of this difference, we have calculated the polarizability value of all the PAHs investigated. The average molecular polarizability is calculated at the M05-2X/6-31G* level, and it is given in Table 5. Remarkably, we find good correlation between the calculated polarizability of the PAHs and the interaction energy value of the complexes in both the cases of L*n* and B*n*. For L*n* systems, the polarizability value ranges from 53.36 to 738.81 au^3 and it increases linearly from L1 to L10. In the case of B*n*, the polarizability value ranges from 140.40 to 568.30 au^3, but there is no linear increase from B3 to B10. The highest value of polarizability is shown for the B6 system, and hence, we can understand why the B6 complexes show higher interaction energy in all the cases. Thus, it appears that the molecular polarizability of the PAHs plays a key role in governing the interaction energy values of the π-complexes.

Shapes and Energies of Frontier Orbitals. We further focus on the interaction energy trend in each chemically different ring of all the systems considered. For instance, in L*n* systems, if we consider L3, the peripheral ring A and central ring B (Scheme 1)

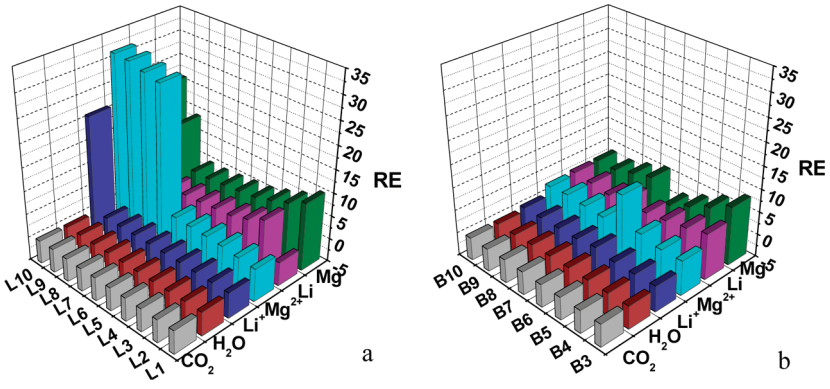

Figure 8. Reorganization energy (kcal/mol) of (a) L*n* and (b) B*n* in the complex formation with CO_2, H_2O, Li^+, Mg^{2+}, Li, and Mg at the M05-2X/6-311++G**//M05-2X/6-31G* level.

dx.doi.org/10.1021/jp201578p |*J. Phys. Chem. C* 2011, 115, 9656–9667

Table 6. Net NPA Charge (amu) on CO_2, H_2O, Li^+, Mg^{2+}, Li, and Mg in the Linear PAH (L*n*) Complexes at the M05-2X/6-311++G//M05-2X/6-31G* Level**

		linear polycyclic aromatic hydrocarbon									
	ring	L1	L2	L3	L4	L5	L6	L7	L8	L9	L10
CO_2	A	−0.001	−0.001	0.023	0.000	0.001	0.002	0.001	0.001	0.002	0.001
	B			0.000	−0.001	0.001	0.001	0.001	0.011	0.000	0.001
	C					0.000	0.003	0.001	0.009	0.002	0.001
	D							−0.001	0.001	0.002	0.000
	E									0.001	0.001
H_2O	A	0.001	0.004	0.005	0.005	0.005	0.005	0.005	0.005	0.005	0.005
	B			0.005	0.005	0.006	0.005	0.005	0.005	0.005	0.005
	C					0.005	0.005	0.003	0.005	0.005	0.005
	D							0.005	0.004	0.004	0.005
	E									0.003	0.003
Li^+	A	0.887	0.900	0.898	0.896	0.895	0.895	0.895	0.894	0.894	0.894
	B			0.914	0.912	0.911	0.910	0.910	0.909	0.909	0.903
	C					0.910	0.908	0.908	0.908	0.907	0.903
	D							0.908	0.906	0.906	0.904
	E									0.905	0.906
Mg^{2+}	A	1.740	1.753	1.756	1.750	1.747	1.744	1.737	1.736	1.735	1.734
	B			1.769	1.765	1.759	1.756	1.756	1.755	1.755	1.752
	C					1.758	1.752	1.750	1.748	1.745	1.189
	D							1.744	1.743	1.740	1.153
	E									1.111	1.132
Li	A	−0.058	0.827	0.848	0.855	0.859	0.861	0.863	0.864	0.865	0.866
	B			0.875	0.880	0.884	0.886	0.886	0.887	0.888	0.885
	C					0.884	0.886	0.888	0.887	0.889	0.888
	D							0.888	0.889	0.889	0.891
	E									0.890	0.893
Mg	A	0.759	0.739	0.766	0.779	0.788	0.794	0.823	0.824	0.824	0.824
	B			0.811	0.812	0.818	0.825	0.824	0.825	0.823	0.743
	C					0.817	0.818	0.823	0.818	0.823	0.806
	D								0.826	0.823	0.805
	E									0.659	0.734

are in different chemical environments. As it could be easily anticipated, the strength of interaction of the complexes formed at each ring with a given metal will be different. This is extending up to the L10 system where there are five such different rings which are named from A to E. Ring A is the peripheral ring in all the cases, but the central ring varies from B to E depending on the size of the system. However, in the case of branched PAHs, since they are not linearly arranged, we have considered only two rings, ring A and ring B, in each case for our study.

As can be seen from Table 3, we have calculated the interaction energy at each different ring of the L*n* systems. In the case of CO_2, as we move from the peripheral ring to the central ring, the interaction energy increases. However, the energy difference between the peripheral and central rings is much less, about 0.2 kcal/mol. A similar energy difference is observed for L*n*−H_2O complexes; however, H_2O shows a preference for peripheral rings, whereas CO_2 shows a preference for the central rings. Since these CO_2 and H_2O are interacting by physisorption, there is no appreciable site preference in the aromatic π-surface. If we considered the case of Li^+, the strength of interaction increases as we move from peripheral to central rings except in the case of L3 (anthracene) where it shows almost similar interaction energy for both peripheral and central rings. Mg^{2+} complexes also show the same trend as their ionic counterpart; i.e., their complex IE is more in the central rings.

Interestingly, in the case of branched systems (B*n*), an opposite trend is shown in most of the cases. However, in CO_2 and H_2O complexes, virtually there is no site preference. Furthermore, in the case of metal atoms and ions in most of the cases, the interaction energy is more in the peripheral rings than the central rings. Hence, it appears that peripheral rings display a stronger property for complexation in the case of branched systems.

In order to understand this behavior, we have calculated the HOMO and LUMO energy values of the L*n* and B*n* systems. Figures 4 and 5 illustrate the orbital pattern and energy of the HOMO and LUMO orbitals of various PAHs considered. The energy of the HOMO orbital increases as the size of the system increases in the case of linear PAHs, and it shows good correlation with the interaction energy of the complexes. Figure 4 shows that, in linear PAH complexes, the HOMO energy values vary from −7.92 to −4.80 eV, while the LUMO energy levels are very close, with energies ranging from −2.47 to

Table 7. Net NPA Charge (amu) on CO_2, H_2O, Li^+, Mg^{2+}, Li, and Mg in the Branched PAH (B*n*) Complexes at the M05-2X/6-311++G**//M05-2X/6-31G* Level

		branched polycyclic aromatic hydrocarbon							
	ring	B3	B4	B5	B6	B7	B8	B9	B10
CO_2	A	0.001	0.000	0.002	0.001	−0.002	−0.001	0.000	0.001
	B	0.000	0.003	0.006	0.002	0.001	0.001	0.001	0.001
H_2O	A	0.004	0.004	0.006	0.000	0.004	0.003	0.004	0.003
	B	0.004	0.003	0.006	0.004	0.006	0.005	0.004	0.006
Li^+	A	0.898	0.902	0.903	0.885	0.910	0.908	0.908	0.908
	B	0.915	0.917	0.926	0.915	0.929	0.927	0.923	0.925
Mg^{2+}	A	1.741	1.750	1.723	1.040	1.762	0.920	1.376	1.754
	B	1.777	1.776	1.752	1.050	1.809	1.800	1.792	1.798
Li	A	0.822	0.861	0.865	0.861	0.879	0.884	0.923	0.887
	B	0.874	0.882	0.909	0.896	0.912	0.910	0.914	0.913
Mg	A	0.743	0.787	0.780	−0.008	0.771	0.768	0.767	0.881
	B	0.728	0.773	0.869	−0.008	0.831	0.773	0.864	0.872

1.16 eV. Next, we will look at the orbital patterns in the case of L*n* systems. In the case of L1 and L2, there is only one type of ring (ring A) and hence we need not consider the orbital distribution between the rings. In the case of L3, the orbital pattern is equally distributed between the rings A and B. However, from L4 to L10, the orbital patterns are concentrated at the central rings than the peripheral rings. This gives us the answer for why the metal atoms and ions show a similar strength of interaction for ring A and ring B in the case of L3 and more interaction at the central rings for the rest of the L*n* systems.

In branched complexes, the HOMO energy values vary from −6.82 to −4.22 eV and the LUMO energy values vary from −0.05 to −2.91 eV. The energies of the HOMO orbitals are in good correlation with the calculated IE values. The highest HOMO energy value is observed for the B6 system, and the calculated IE is also the highest for the same. The orbital patterns of the B*n* systems primarily reside on the peripheral regions, and thus, it gives the answer for why the strength of interaction is more in the peripheral rings in the case of B*n* complexes. Thus, the HOMO energy value and the orbital distribution seem to be good evidence to explain the strength of interaction of the π complexes of graphene nanoflakes. However, this is only a qualitative measure. In order to get quantitative evidence, we have done the NICS value calculation.

Nucleus Independent Chemical Shift (NICS). The calculated NICS values for L*n* and B*n* systems are given in Tables S3 and S4 in the Supporting Information. If we considered L*n* systems, as the size of the system increases, the NICS value of the peripheral rings decreases and the central ring increases. As the negative NICS shows aromaticity, it appears that as we move from L1 to L10 the aromaticity decreases in the peripheral rings and it increases in the central rings. On the whole, the aromaticity is more at the central rings than the peripheral rings. Figures 6 and 7 shows the comparison of the trend in IE of various complexes with the trend in the calculated NICS value. If we move from ring A to the central rings in each case, the NICS value increases. The same trend is shown by the binding energy values of the π complexes in the L*n* system in most of the cases. However, in the case of the L10 system, the trend is slightly away from the NICS values as the PAHs undergo more deformation during their complex formation.

Table 8. M05-2X/6-31G* Level C−H Bending (out of plane) Frequency of Representative L*n* and B*n* Complexes (for Full Detail, See Supporting Information Table S8)

L*n*	C−H bending (cm^{-1})	B*n*	C−H bending (cm^{-1})
L1	696	B3	764
L1_CO_2	701	B3_CO_2	766
L1_H_2O	711	B3_H_2O	771
L1_Li^+	753	B3_Li^+	795
L1_Mg^{2+}	810	B3_Mg^{2+}	793
L1_Li	726	B3_Li	714
L1_Mg	781	B3_Mg	738
L2	817	B5	845
L2_CO_2	817	B5_CO_2	845
L2_H_2O	826	B5_H_2O	847
L2_Li^+	850	B5_Li^+	858
L2_Mg^{2+}	879	B5_Mg^{2+}	868
L2_Li	784	B5_Li	816
L2_Mg	785	B5_Mg	798
L5	946	B6	745
L5_CO_2	945	B6_CO_2	754
L5_H_2O	949	B6_H_2O	762
L5_Li^+	963	B6_Li^+	783
L5_Mg^{2+}	965	B6_Mg^{2+}	797
L5_Li	915	B6_Li	757
L5_Mg	896	B6_Mg	765
L10	953	B10	924
L10_CO_2	953	B10_CO_2	923
L10_H_2O	955	B10_H_2O	926
L10_Li^+	959	B10_Li^+	937
L10_Mg^{2+}	979	B10_Mg^{2+}	949
L10_Li	931	B10_Li	889
L10_Mg	933	B10_Mg	894

Similarly, in the branched systems, the NICS value is more at the peripheral rings than at the central rings and the same trend is shown in the strength of interaction of their π complexes in most of the cases.

Reorganization Energy (RE) and Charge Transfer. In order to analyze the strain induced in the PAH structures upon complexation, the reorganization energy is calculated. A plot of the RE as a function of the size of the system for all the complexes considered in this study is shown in Figure 8. It is shown from the figure that there is no significant strain occurring in the case of CO_2 and H_2O complexes. This is more evidence for the fact that CO_2 and H_2O interact on the graphene surface by physisorption rather than chemisorption. However, metal and ions induce an appreciable strain in the PAHs. Linear PAHs are more strained due to metal ion complexation than the branched PAHs, and among the linear PAHs, L10 has undergone more deformation and thus their IE trends vary from the rest of the systems.

The charge transfer that occurred during the complex formation is calculated at the M05-2X/6-311++G**//M05-2X/6-31G* level of theory. Tables 6 and 7 illustrate the net charge present on the complex counterparts. As one could easily predict, there is no significant charge transfer occurring in the case of CO_2 and H_2O complexes. However, there is appreciable charge transfer in the case of metal atoms and ions. The charge on the Li^+ ion has changed from 1 to 0.800 amu, and the charge on

Mg^{2+} has changed from 2 to 1.7 amu; this indicates that a notable charge has been transferred from the aromatic surface to the metal ions. Similarly, in the case of neutral atoms, it is 0−0.8 and 0−0.7 amu, respectively, for Li and Mg. The positive charge on the neutral atoms in the complexed state shows that charge has been transferred from the alkali metals to the aromatic surface.

Vibrational Analysis. Spectroscopic signatures will be of great importance in experimentally validating the computational results. In PAHs, the characteristic modes occur in the low frequency range between 900 and 675 cm^{-1}. These high intensity bands result from the out-of-plane bending of the ring C−H bonds. Hence, we are interested in the C−H bending frequencies of various L*n* and B*n* complexes. Table 8 shows the variation in the C−H bending frequency upon complex formation. The other characteristic absorption data of PAHs such as C−H stretching, C−H bending, and C−C stretching were provided in the Supporting Information (Tables S7 and S8). Virtually, there is no change in the C−H bending frequency in the case of CO_2 and H_2O; however, the metal ion complexes show a blue shift, while the neutral metal atom complexes show a red shift. The shifts in the vibrational frequencies of PAH upon complex formation with various atoms, molecules, and ions have been computed using the M05-2X/6-31G* level of theory.

CONCLUSIONS

The binding energy and conformational preference of CO_2, H_2O, Li^+, Mg^{2+}, Li, and Mg have been comprehensively analyzed on a range of model systems, L*n* and B*n*, aimed to mimic the truncated graphene sheets. CO_2 is oriented parallel above the PAH surface, whereas H_2O is oriented above PAHs such that the two H atoms are pointing toward the ring. Alkali and alkaline earth metal atoms and ions are oriented exactly above the center of the six membered ring in PAHs. CO_2 and H_2O interact with the PAH surfaces by physisorption, whereas the metal atoms and ions interact by chemisorption. The binding energy varies linearly as the size of the system increases in the case of L*n*, but there is no such linear variation in the case of B*n*. The HOMO energy and polarizability of PAHs play an important role in determining the strength of interaction. The preferred site of orientation of metal atoms and ions in linear and branched PAHs are different such that the peripheral rings are more occupied in the case of branched systems, whereas the central rings are more occupied in the case of linear systems. The origin of this difference can be explained by the calculated NICS value and the HOMO pattern of the different sites in the PAHs.

ASSOCIATED CONTENT

Supporting Information. The interaction energy values obtained at the M05-2X/6-31G* level of all the complexes considered; NICS value of PAHs at the M05-2X/6-31G* level; reorganization energy values at the M05-2X/6-311++G**//M05-2X/6-31G* level; vibrational frequencies of L*n* and B*n* complexes at the M05-2X/6-31G* level; and IE of L*n* and B*n* complexes with and without BSSE correction. This material is available free of charge via the Internet at http://pubs.acs.org.

AUTHOR INFORMATION

Corresponding Author

*Phone: +91 40 27193016. Fax: +91 40 27160512. E-mail: gnsastry@gmail.com.

ACKNOWLEDGMENT

D.U. thanks CSIR, New Delhi, for financial assistance, and G.N.S. thanks DST Swarnajayanthi Fellowship and India European collaboration project AMCOS for supporting this research.

REFERENCES

(1) Allen, M. J.; Tung, V. C.; Kaner, R. B. *Chem. Rev.* **2010**, *110*, 132–145.

(2) (a) Stoller, M. D.; Park, S.; Zhu, Y.; An, J.; Ruoff, R. S. *Nano Lett.* **2008**, *8*, 3498–3502. (b) Si, Y.; Samulski, E. T. *Chem. Mater.* **2008**, *20*, 6792–6797. (c) Pumera, M.; Ambrosi, A.; Bonanni, A.; Khim Chng, E. L.; Poh, H. L. *Trends Anal. Chem.* **2010**, *29*, 954–965.

(3) (a) Chen, L.; Cooper, A. C.; Pez, G. P.; Cheng, H. *J. Phys. Chem. C* **2007**, *111*, 18995–19000. (b) Denis, P. A.; Iribarne, F. *THEOCHEM* **2009**, *907*, 93–103. (c) Rubes, M.; Bludsky, O. *ChemPhysChem* **2009**, *10*, 1868–1873.

(4) Ritter, K. A.; Lyding, J. W. *Nat. Mater.* **2009**, *8*, 235–242.

(5) (a) Tang, S.; Cao, Z. *J. Chem. Phys.* **2011**, *134*, 044710–14. (b) Wang, Y.; Shao, Y.; Matson, D. W.; Li, J.; Lin, Y. *ACS Nano* **2010**, *4*, 1790–1798.

(6) (a) Rao, C. N. R.; Sood, A. K.; Subrahmanyam, K. S.; Govindaraj, A. *Angew. Chem., Int. Ed.* **2009**, *48*, 7752–7777. (b) Schedin, F.; Geim, A. K.; Morozov, S. V.; Hill, E. W.; Blake, P.; Katsnelson, M. I.; Novoselov, K. S. *Nat. Mater.* **2007**, *6*, 652–655.

(7) Al-Mashat, L.; Shin, K.; Kalantar-zadeh, K.; Plessis, J. D.; Han, S. H.; Kojima, R. W.; Kaner, R. D.; Li, D.; Gou, X.; Ippolito, S. J.; Wlodarski, W. *J. Phys. Chem. C* **2010**, *114*, 16168–16173.

(8) (a) Lee, G.; Lee, B.; Kim, J.; Cho, K. *J. Phys. Chem. C* **2009**, *113*, 14225–14229. (b) Valencia, H.; Gil, A.; Frapper, G. *J. Phys. Chem. C* **2010**, *114*, 14141–14153. (c) Ghaderi, N.; Peressi, M. *J. Phys. Chem. C* **2010**, *114*, 21625–21630.

(9) (a) Park, S.; Lee, K.; Bozoklu, G.; Cai, W.; Nguyen, S. T.; Ruoff, R. S. *ACS Nano* **2008**, *2*, 572–578. (b) Wang, D.; Kou, R.; Choi, D.; Yang, Z.; Nie, Z.; Li, J.; Saraf, L. V.; Hu, D.; Zhang, J.; Graff, G. L.; Liu, J.; Pope, M. A.; Aksay., I. A. *ACS Nano* **2010**, *4*, 1587–1595. (c) Quintana, M.; Spyrou, K.; Grzelczak, M.; Browne, W. R.; Rudolf, P.; Prato, M. *ACS Nano* **2010**, *4*, 3527–3533. (d) Tachikawa, H.; Iyama, T. *Jpn. J. Appl. Phys.* **2010**, *49*, 06GJ12−4. (e) Al-Aqtash, N.; Vasiliev, I. *J. Phys. Chem. C* **2009**, *113*, 12970–12975.

(10) (a) Kuc, A.; Heine, T.; Seifert, G. *Phys. Rev. B* **2010**, *81*, 085430–7. (b) Rieger, R.; Mullen, K. *J. Phys. Org. Chem.* **2010**, *23*, 315–325.

(11) (a) Podeszwa, R. *J. Chem. Phys.* **2010**, *132*, 044704–8. (b) Northrop, B. H.; Norton, J. E.; Houk, K. N. *J. Am. Chem. Soc.* **2007**, *129*, 6536–6546.

(12) (a) Pollak, E.; Geng, B.; Jeon, K.; Lucas, I. T.; Richardson, T. J.; Wang, F.; Kostecki, R. *Nano Lett.* **2010**, *10*, 3386–3388. (b) Tachikawa, H.; Nagoya, Y.; Fukuzumi, T. *J. Power Sources* **2010**, *195*, 6148–6152.

(13) (a) Reddy, A. S.; Sastry, G. M.; Sastry, G. N. *Proteins: Struct., Funct., Bioinf.* **2007**, *67*, 1179–1184. (b) Reddy, A. S.; Sastry, G. N. *J. Phys. Chem. A* **2005**, *109*, 8893–8903.

(14) (a) Vijay, D.; Sastry, G. N. *Phys. Chem. Chem. Phys.* **2008**, *10*, 582–590. (b) Priyakumar, U. D.; Sastry, G. N. *Tetrahedron Lett.* **2003**, *44*, 6043–6046. (c) Priyakumar, U. D.; Punnagai, M.; Krishna Mohan, G. P.; Sastry, G. N. *Tetrahedron* **2004**, *60*, 3037–3043. (d) Gal, J.; Maria, P.; Decouzon, M.; Mo, O.; Yanez, M.; Abboud, J. L. M. *J. Am. Chem. Soc.* **2003**, *125*, 10394–10401.

(15) (a) Reddy, A. S.; Zipse, H.; Sastry, G. N. *J. Phys. Chem. B* **2007**, *111*, 11546–11553. (b) Rao, J. S.; Zipse, H.; Sastry, G. N. *J. Phys. Chem. B* **2009**, *113*, 7225–7236.

(16) (a) Kolesnikov, A. I.; Zanotti, J. M.; Loong, C. K.; Thiyagarajan, P.; Moravsky, A. P.; Loutfy, R. O.; Burnham, C. J. *Phys. Rev. Lett.* **2004**, *93*, 035503–4. (b) Ghosh, A.; Subrahmanyam, K. S.; Krishna, K. S.; Datta, S.; Govindaraj, A.; Pati, S. K.; Rao, C. N. R. *J. Phys. Chem. C* **2008**, *112*, 15704–15707.

(17) Liu, Z.; Robinson, J. T.; Sun, X.; Dai, H. *J. Am. Chem. Soc.* **2008**, *130*, 10876–10877.

(18) (a) Varghese, N.; Mogera, U.; Govindaraj, A.; Das, A.; Maiti, P. K.; Sood, A. K.; Rao, C. N. R. *ChemPhysChem* **2009**, *10*, 206–210. (b) Qin, W; Li, X.; Bian, W.; Fan, X.; Qi, J. *Biomaterials* **2010**, *31*, 1007–1016. (c) Rajesh, C.; Majumder, C.; Mizuseki, H.; Kawazoe, Y. *J. Chem. Phys.* **2009**, *130*, 124911–6. (d) Sheng, L.; Ono, Y.; Taketsugu, T. *J. Phys. Chem. C* **2010**, *114*, 3544–3548.

(19) Hohenstein, E. G.; Chill, S. T.; Sherrill, C. D. *J. Chem. Theory Comput.* **2008**, *4*, 1996–2000.

(20) (a) Portella, G.; Poater, J.; Bofill, J. M.; Alemany, P.; Sola, M. *J. Org. Chem.* **2005**, *70*, 2509–2521. (b) Saieswari, A.; Priyakumar, U. D.; Sastry, G. N. *THEOCHEM* **2003**, *663*, 145–148.

(21) Lu, Y.; Lee, S. *Int. J. Quantum Chem.* **1992**, *44*, 773–784.

(22) Reed, A. E.; Curtiss, L. A.; Weinhold, F. *Chem. Rev.* **1988**, *88*, 899–926.

(23) Frisch, M. J.; Trucks, G. W.; Schlegel, H. B.; Scuseria,G. E.; Robb, M. A.; Cheeseman, J. R.; Montgomery, J. A.; Vreven, T., Jr.; Kudin, K. N.; Burant, J. C.; Millam, J. M.; Iyengar, S. S.; Tomasi, J.; Barone, V.; Mennucci, B.; Cossi, M.; Scalmani, G.; Rega, C.; Petersson, G. A.; Nakatsuji, H.; Hada, M.; Ehara, M.; Toyota, K.; Fukuda, R.; Hasegawa, J.; Ishida, M.; Nakajima, T.; Honda, Y.; Kitao, O.; Nakai, H.; Klene, M.; Knox, X.; Li, J. E.; Hratchian, H. P.; Cross, J. B.; Adamo, C.; Jaramillo, J.; Gomperts, R.; Stratmann, R. E.; Yazyev, O.; Austin, A. J.; Cammi, R.; Pomelli, C.; Ochterski, J. W.; Ayala, P. Y.; Morokuma, K.; Voth, G. A.; Salvador, P.; Dannenberg, J. J.; Zakrzewski, V. G.; Dapprich, S.;. Daniels, A. D.; Strain, M. C.; Farkas, O.; Malick, D. K.; Rabuck, A. D.; Raghavachari, K.; Foresman, J. B.; Ortiz, J. V.; Cui, Q.; Baboul, A. G.; Clifford, S.; Cioslowski, J.;. Stefanov, B. B.; Liu, G.; Liashenko, A.; Piskorz, P.;. Komaromi, I.; Martin, R. L.; Fox, D. J.; Keith, T.; Al-Laham, M. A.; Peng, C. Y.; Nanayakkara, A.; Challacombe, M.; Gill, P. M. W.; Johnson, B.; Chen, W.; Wong, M. W.; Gonzalez, C.; Pople, J. A. *Gaussian 03*, revision E.1; Gaussian, Inc.: Pittsburgh, PA, 2003.

(24) Lan, J.; Cao, D.; Wang, W.; Smit, B. *ACS Nano* **2010**, *4*, 4225–4237.